Composites: Part A 150 (2021) 106627

Contents lists available at ScienceDirect

Composites Part A

journal homepage: www.elsevier.com/locate/compositesa

Delamination suppression in tapered unidirectional laminates with multiple ply drops using a tape scarfing technique

Tharan Gordon [a], Xiaodong Xu [a,b], Luiz Kawashita [a], Michael R. Wisnom [a], Stephen R. Hallett [a], Byung Chul Kim [a,*]

[a] Bristol Composites Institute (ACCIS), Advanced Composites Collaboration for Innovation and Science, University of Bristol BS8 1TR, United Kingdom
[b] University of the West of England, Coldharbour Lane, Bristol BS16 1QY, United Kingdom

ARTICLE INFO

Keywords:
Prepreg
Ply-drop
Delamination
Automated Fibre Placement (AFP)
Cutting

ABSTRACT

Composite laminate thickness tapering is essential for weight efficient structures. This is achieved by terminating specific plies, but these can in turn act as sites for delamination initiation. One area of importance is the spacing between adjacent ply drops, which can have a significant impact on the delamination stress. In this work, a novel tape scarfing method that applies a tapered profile to dropped ply ends was used on unidirectional tapered laminate specimens with multiple ply drops. The effect of ply drop spacing on the delamination stress of both conventional and scarfed plies in tension was studied experimentally. The results showed that the scarfed ply drop configurations can completely suppress delamination in certain configurations. The scarfed ply drops also retained higher performance with smaller ply drop spacings. This indicates that in using scarfed plies, conventional laminate design rules could be relaxed and the weight of the structure could be further reduced. The underlying failure mechanisms were also investigated using both analytical and numerical methods. A simple stress-based formula for estimating the delamination stress of scarfed plies was introduced and shown to be consistent with both experimental and numerical results, which could be used (and further developed) to make tapered laminate design easier.

1. Introduction

Within large aircraft laminated composite material components, there are likely to be a multitude of ply drops present at a variety of distances from one another, to achieve a weight efficient structural performance. Ply drops in fibre reinforced composites are well understood to have a negative impact on failure loads, owing to their tendency to act as zones of delamination onset [1]. Effort has been made previously to characterise the relationship between successive ply drop-off spacing or staggering distance ($\Delta_{\text{ply-drop}}$ in Fig. 1) and laminate delamination behaviour. This parameter is of interest to understand for a number of reasons: it has a bearing on the required accuracy of the manufacturing method employed for a certifiable strength of component and it may impose a design constraint on how quickly a thick pad up region for example, can be tapered down to a thinner one.

Cui et al. [2] tested multiple arrangements of unidirectional, symmetrically tapered laminates with a variety of ply drop-off spacings ranging from 0 to 2 mm and found the existence of a critical value, above which interaction between successive ply drops is negligible. Below this critical value of ply drop spacing, they were found to interact, leading to a decrease in the delamination onset stress of the tested samples. Most of the interaction was found to occur within a relatively small range of spacings, with the maximum delamination stress found to be about 27% lower than that for the non-interacting ply drops. The authors proposed the following simple formula to estimate the critical interaction distance, S_c assuming a linear relationship between delamination stress and spacing:

$$S_C = \frac{\sigma t}{2\tau_y} \tag{1}$$

where σ is the fibre direction stress in the dropped ply, t is the thickness of the dropped ply and τ_y is the shear yield stress. The method solely considered an axially loaded sample and was later further expanded by Allegri et al. [3] using extended shear lag theory to incorporate mixed axial/bending load cases. Mukherjee et al. [4] added to this line of work by conducting numerical simulations of varying ply drop spacing distances and fibre orientations of the dropped plies, and confirmed the presence of a critical distance as previously described. They noted that

* Corresponding author.

https://doi.org/10.1016/j.compositesa.2021.106627
Received 22 March 2021; Received in revised form 27 June 2021; Accepted 19 August 2021
Available online 26 August 2021

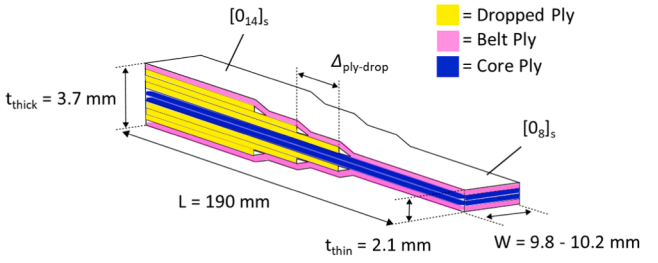

Fig. 1. Schematic of the specimens tested experimentally in this work, including stacking sequence and average coupon dimensions.

there was a dependency on the fibre orientation of the dropped plies, which determines the in-plane stiffness and hence load carried in those plies; plies where the fibres are orientated to the loading direction required the largest critical distance to nullify interaction. One method of preventing the interaction between adjacent ply drops is thus to separate the adjacent ply drops to a distance greater than the critical distance, and therefore impose a constraint on the possible taper ratio and sacrifice weight efficiency. Another approach is to interleave adjacent ply drops between continuous plies, which has been widely studied e.g. [5]. This approach is considered to be effective in industry, however, the complexity of the design process required can present a major challenge. A method of reducing the localised stress discontinuity by applying a chamfer to the dropped ply end has been shown to successfully suppress delamination for multiple laminate configurations [6]. However, the chamfering technique used (i.e. abrasive machining) appeared unlikely to be practical for industrial implementation, and the effects of any interaction among adjacent chamfered plies and its impact on delamination onset was not investigated in detail.

Recently, a novel tape termination method suitable for automated fibre placement (AFP) machines has been developed [7,8], which can apply an accurate chamfer to the dropped ply end in a process referred to as 'tape scarfing'. The method was experimentally demonstrated to completely suppress delamination in unidirectional laminates with a single ply drop loaded in tension.

This paper investigates the effect of ply drop spacing on the delamination stress of scarfed plies and contrasts it to conventional ply drops. To investigate the influence of ply drop spacing, quasi-static tensile tests were conducted on unidirectional tapered laminates with three internal plies successively terminated by the conventional cut and tape scarfing methods. The delamination behaviour of each specimen was captured using a high-speed camera. Furthermore, a simple analytical formula was then proposed for estimating the delamination stress of the scarfed ply specimens, paving the way for easy laminate design in the future. Finite element analyses were also conducted to provide a more in-depth understanding of the delamination mechanism as well as the internal stress distributions, which could be used to improve upon the simple analytical method proposed. The ply scarfing technique was shown to be able to completely suppress delamination and enable the use of reduced ply drop spacing required when tapering laminates.

2. Sample preparation and test method

Six different configurations of unidirectional and symmetrically tapered laminate specimens were tested (see Figs. 2 and 3). In each

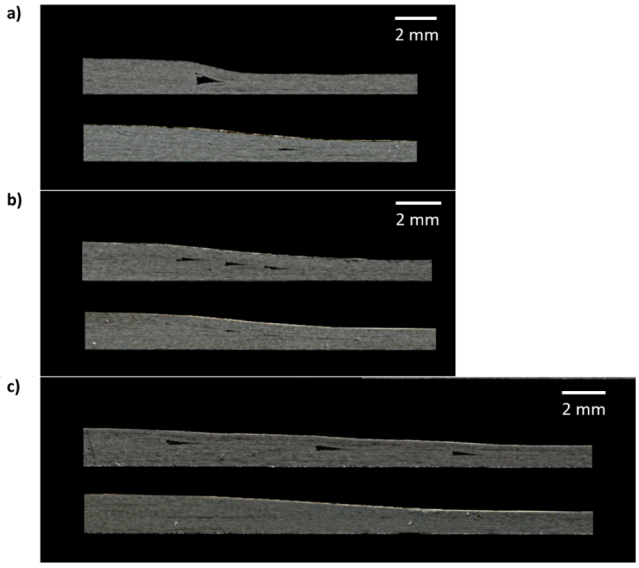

Fig. 3. Cross sectional images of the test specimens, with conventional ply drops on top and scarfed plies bottom: (a) 0 mm ply drop spacing, (b) 2 mm ply drop spacing, and (c) 5 mm ply drop spacing.

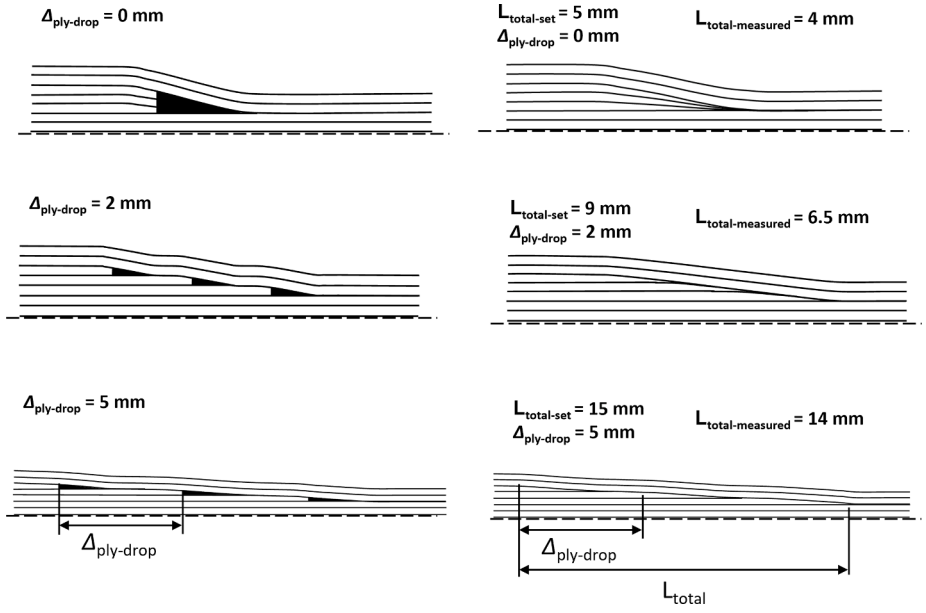

Fig. 2. Half schematics of each series of test coupons included in the experimental tests, with nominal values of the total tapered region included for each.

configuration, 6 pairs of blocked plies were dropped symmetrically about the midplane of the specimens, with 3 different ply drop spacings of 0 mm, 2 mm and 5 mm. Whilst $\Delta_{\text{ply-drop}}$ is not the only way to describe the tapered portion of the specimens, it was chosen as it is the only parameter that we could control in the manufacturing process. It is also a parameter that is commonly used in the aerospace industry during the detailed design and manufacturing stages as well as in academic papers. Two termination methods were used for direct comparison – conventional ply termination as currently employed in AFP machines and the novel tape scarfing method. A 1:20 scarfing ratio was used for each scarfed ply drop regardless of the spacing distance as this ratio has been demonstrated to completely suppress delamination in a single ply drop sample [8]. This choice of spacing resulted in overlap of successive scarfed ply ends at 0 mm and 2 mm spacing, as shown schematically in Fig. 2.

Each 240 mm× 210 mm test panel was made using a carbon fibre/epoxy prepreg (IM7/8552, Hexcel, US) which has a nominal ply thickness, t_{ply} of approximately 0.131 mm when cured. Blocked plies comprising two prepreg sheets were used for the lay-up. For the scarfed discontinuous plies, strips of 24 mm wide blocked plies were scarfed using a bespoke test rig as described in detail in Ref [8]. Laminates were produced on a flat aluminium tool plate with no top tooling present, yielding asymmetrically tapered panels and were cured following the manufacturer's recommended cure cycle (2 h at 180 °C, at 7 bar gauge pressure). 10 mm from the cured plate edges was trimmed, and each panel was cut in half and bonded back-to-back using an epoxy paste adhesive (Araldite 2014–1, Huntsman, US), resulting in a symmetrically tapered panel. Prior to bonding, the flat surface was prepared using 150-grit sandpaper, and the ply drop locations were identified by visually inspecting the cut edge to aid in alignment of the ply drops. 50 mm long and 2 mm thick glass–epoxy end tabs were bonded to the specimen ends using the same adhesive and the whole assembly was oven cured at 80 °C for 1 h. The bonded panels were cut into 10 mm wide symmetrically tapered coupons using a precision diamond wheel cutter. The average total length of each coupon was 190 mm, with a gauge length of 90 mm. Excluding the adhesive thickness which had some variability, the thin section had a nominal laminate thickness of 2.1 mm (based on the cured ply thickness of 0.131 mm), and the thick section nominal laminate thickness was 3.7 mm – see Fig. 1. The adhesive layer was quite thick in some cases (approximately 0.5 mm), however, it was ignored in the nominal thickness specification as used later for calculations, as there was no significant influence on the delamination onset stress.

Fig. 3 shows the representative images of half of the untested specimens. For the conventional ply drop specimens, the ply drop spacings were in good agreement with the as-designed configurations. In each case, the resin pocket at the terminated ply end was easy to distinguish, and each sample was symmetric about the bond line. There was some consolidation effect at the terminated ply end resulting in slightly smaller thickness steps than the nominal ply thickness.

For the scarfed ply drop specimens, both the 2 mm and the 5 mm spacing samples had no distinct feature at the terminated ply. In the case of the 0 mm spacing sample, a small resin pocket was formed at the terminated ply end owing to the stiffness of the belt plies and the high level of ply overlap. The external geometry of the scarfed ply and conventionally dropped samples in the 2 mm and 5 mm spacing cases matched well, with the 0 mm spacing case having a lower taper angle owing to the absence of clear discontinuous steps within the sample.

Tensile tests were carried out using a 250 kN servo-hydraulic test machine, under displacement control with a crosshead speed of 1 mm/min. A minimum of four specimens were tested in each case. Delamination onset and the dominant failure mode were captured using a high-speed camera (Fastcam SA-Z, Photron, JP) at a frame rate of 280,000 fps.

3. Experimental results

3.1. Conventional ply drop failure behaviour

All the conventional specimens failed by delamination. Fig. 4 shows two representative load–displacement curves with the minimum and maximum delamination onset loads for each case. All delamination events corresponded to a sharp load drop taken from the test machine – such as has been previously seen in Ref. [8]. For clarity in each case, the plot has been terminated before complete catastrophic failure of the samples and highlights only the first failure Arrows are included to clearly indicate the delamination onset loads. The nonlinearity is an artifact from small amounts of specimen slippage in the test machine grips. The high-speed camera clearly captured the delamination onset, as shown in the successive frames included in Figs. 5–7. However, the propagation of the delamination was of such rapidity that there was difficulty in identifying the exact initiation site of any delamination. When the crack propagated, each set of ply drops about the line of symmetry was seen to have delaminated at approximately the same time.

For the 0 mm spacing samples, a prominent delamination in the thin section of the samples was present between the continuous core and belt plies (defined in Fig. 1), that extended into the thin section of the specimen but did not reach the end tabs. Thick section delamination between the entire discontinuous block of plies, and the surrounding continuous core and belt plies was also present in all the 0 mm spacing samples and propagated along the whole specimen length to the end tabs.

As the ply drop spacing became larger, the specimens showed a decreased likelihood of thin section delamination. The failure behaviour of the 0 mm spacing samples was a mixture of thin and thick section delamination, with prominent thin section delamination in all cases. The same behaviour was also observed in the 2 mm spacing cases, although the thin section delamination was only present in some, not all, test cases, implying that both failure modes were in competition in this configuration. The load at which both the 0 mm and 2 mm spacing samples delaminated was approximately the same (31.7 ± 5.3 kN and 31.3 ± 1.4 kN respectively). It is worth noting that 0 mm spacing specimens had a significantly larger variation in the delamination onset stress, which is potentially due to the local variability of the resin pocket geometry [9]. The 5 mm spacing specimens failed at 45.7 kN, by delaminating solely into the thick section of the specimen from the ply drop closest to the core plies, which is shown in (Fig. 7(a)).

From Equation (1), considering the point at which the thin section stress reaches the material failure stress (2724 MPa [10]), the stress in

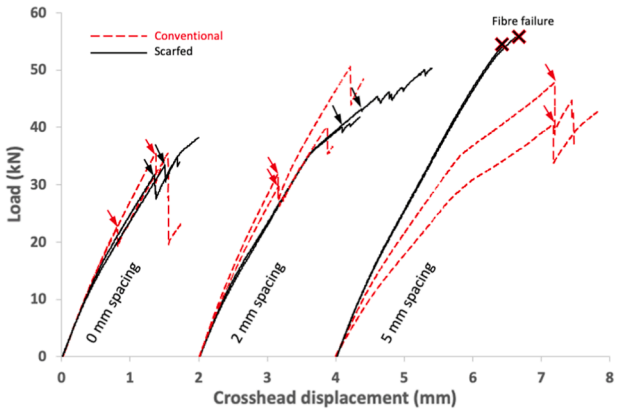

Fig. 4. Representative load vs. crosshead displacement plots with delamination onset points indicated with arrows. (The stiffness change was due to the slippage of the specimens during the tests.) Some of the tests were stopped prior to ultimate failure.

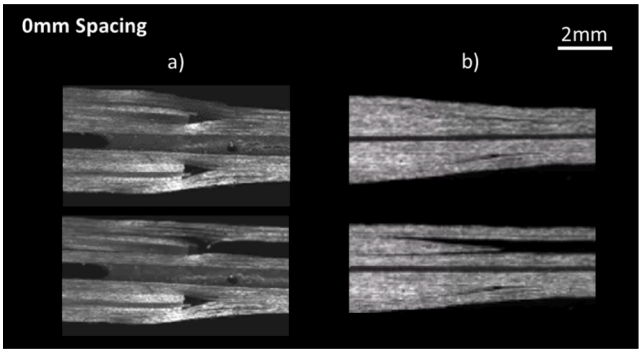

Fig. 5. high speed images corresponding to the coupon's pre-failure (top) and post-failure (bottom): (a) 0 mm spacing conventional sample, and (b) 0 mm spacing scarfed sample.

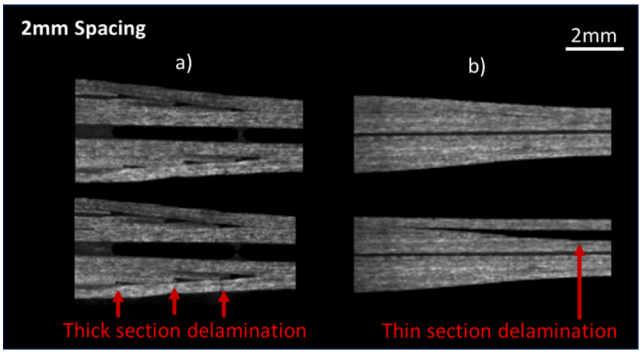

Fig. 6. High speed images corresponding to the coupon's pre-failure (top) and post-failure (bottom): (a) 2 mm spacing conventional sample, and (b) 2 mm spacing scarfed sample.

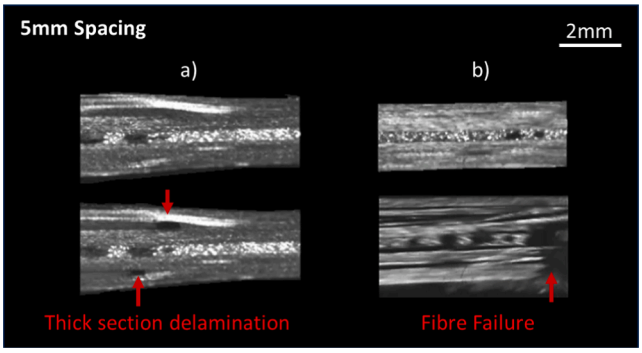

Fig. 7. High speed images corresponding to the coupon's pre-failure (top) and post-failure (bottom): (a) 5 mm spacing conventional sample, and (b) 5 mm spacing scarfed sample – flat region just ahead of taper.

the thicker portion of the sample past the first dropped block ply, σ, is given by $2724 \times t_{thin} / (t_{thin} + 2t_{ply}) = 2180$ MPa. Using this value, along with the shear yield stress of the composite, τ_y (82.5 MPa [11]), the critical distance of conventional ply drop interaction, S_c, is estimated to be approximately 3.4 mm in the current samples. This value is consistent with the experimental observations: it is below the 5 mm spacing, which saw the absence of ply drop interaction and had approximately the same delamination onset stress as that of a specimen with a single ply drop (2238 versus 2376 MPa [8]), and above the 2 mm spacing which saw a performance knockdown to 1491 MPa.

3.2. Scarfed ply drop failure behaviour

As shown in Fig. 5 (b), the 0 mm spacing samples displayed a prominent thin section delamination at the point of failure, with separation between the continuous belt and core plies, along with some thick section delamination. Both the location of crack growth and the delamination stress were approximately the same for this configuration as for the conventionally dropped specimens. However, it is worth noting that the variation in the delamination stress was significantly lower than that of the conventionally dropped specimens, as shown in Fig. 8, which also includes the single ply drop results from [8].

The 2 mm spacing scarfed samples were also observed to fail by delamination. This was visible in high speed footage (Fig. 6 (b)) along with clear load drops in the force–displacement data (Fig. 4). The delamination was rapid and the location varied from sample to sample; some specimens exhibited peel stress dominated thin section delamination, whereas others showed only shear dominated thick section delamination, which indicates competition between those two failure modes, as was the case for the conventional specimens. Due to the high crack propagation speed, it was not possible to determine which delamination occurred first or whether the competing failure modes occurred simultaneously.

In contrast to the 0 mm and 2 mm spacing samples, the scarfed 5 mm ply drop spacing samples did not delaminate and were observed to fail catastrophically by fibre failure in the thin section, as shown in Fig. 7 (b), just ahead of the tapered region. Up until the point of failure there was nothing observable in high speed footage or load–displacement curves (Fig. 4) to suggest alternative damage mechanisms taking place. The average load reached before failure was 55.1 kN.

3.3. Discussion of failure

A summary plot of the experimental failure loads is shown in Fig. 8 and tabulated as stresses in the thin section, based on the nominal laminate thickness and actual sample widths in Table 1. At 0 mm ply drop spacing, both scarfed and conventional configurations displayed significant thin section delamination at failure along with delamination into the thick section. In both cases, the average failure stress of ~ 1510 MPa was approximately the same, however this may be coincidental. The conventional specimens at 0 mm exhibited a larger scatter, which is likely due to the greater manufacturing variability when terminating the plies conventionally. With multiple plies dropped at a single station, the sharply terminated ply ends have the potential to be misaligned. Further to this, because of using soft top tooling the taper angle at the ply drops (influencing the angle of the belt ply) could also be more inconsistent for the conventional specimens than the scarfed (which have a more well-defined geometry). This variability could significantly affect the

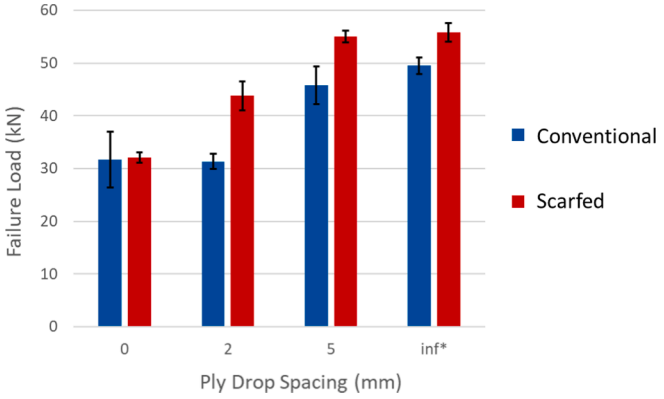

Fig. 8. Bar chart showing the average experimental failure load of all specimens tested. *inf refers to single ply drop specimens tested previously in Ref. [8].

Table 1
Failure load for each set of experimental results, along with its conversion to thin section failure stress.

Sample Type	Spacing (mm)	Failure load (kN)	*CV (%)*	Thin section Failure stress (MPa)	*CV (%)*	Delamination mode
Scarfed	**0**	**32.08**	*2.96*	**1511**	*3.07*	Thin + Thick section
	2	**43.77**	*6.30*	**2064**	*6.17*	Thin + Thick section
	5	**55.08**	*1.98*	**2611**	*1.12*	Fibre failure
	∞ [8]	**55.83**	*3.15*	**2612**	*3.39*	Fibre failure
Conventional	**0**	**31.66**	*16.69*	**1511**	*16.69*	Thin + Thick section
	2	**31.32**	*4.55*	**1491**	*3.93*	Thin + Thick section
	5	**45.74**	*7.80*	**2238**	*7.47*	Thick section
	∞ [8]	**49.51**	*3.15*	**2376**	*3.47*	Thick section

delamination stress.

At 2 mm ply drop spacing, the scarfed ply specimens showed a clear increase in delamination stress compared to 0 mm spacing. As indicated in Table 1, the mode of failure was mixed, with thick section delamination in all samples accompanied by thin section delamination in some. The variability of the delamination direction in each case is an indication of two different factors driving failure: the transfer of stress carried in the discontinuous plies (scarfed or conventional) to the continuous, and the through-thickness stresses owing to the tapered geometry in the sample, which increases the likelihood of thin section delamination at steeper angles owing to increased peel stresses in the belt plies [9,12]. Whilst still undergoing delamination, the scarfed ply drop specimens of 2 mm spacing delaminated at an average thin-section stress of 2064 MPa, which is 38.5% higher than the conventional ply drop specimens' of 1491 MPa.

For the scarfed ply samples, there was clearly a more gradual reduction in the delamination stresses with decreased ply drop spacing, as shown in Fig. 8. This behaviour not only indicates ply scarfing results in stronger, more delamination resistant specimens, but also that the method will be more tolerant of inaccuracies in ply drop spacing during manufacturing, in that the strength knockdown with spacing was more gradual and therefore is less sensitive to small misalignments. As an example of such misalignments, the tolerance of on-the-fly AFP cutting is known to be of the order of approximately 1.5 mm [13,14].

Prior tests conducted on single ply drop specimens [8] with the same belt and core laminate thicknesses as those currently tested effectively serve as a proxy for infinitely spaced multiple ply drop specimens [15]. At 5 mm ply drop spacing, the delamination onset stresses of the conventionally dropped specimens were almost the same as the infinite spacing ones, which is indicative of a lack of interaction between adjacent ply drops. Although the mean delamination stress appears slightly lower than that of the single ply drop conventional specimens reported (infinite spacing in Table 1), the scatter bars overlap indicating a lack of statistical difference. As well as similar failure stress, the same failure mode was observed, as expected from Equation (1), as the ply drops are spaced further apart than their critical interaction distance. Performing similarly, the scarfed ply specimens at 5 mm spacing also exhibited no sign of interaction between adjacent ply terminations. They exhibited a clear suppression of delamination and failed by fibre failure at 2612 MPa, while the conventionally dropped samples delaminated into the thick section at 2238 MPa. This represents an increase in failure stress of approximately 17% when terminating the plies with the tape scarfing method.

The increase in delamination stress further attests to the ultimate performance benefit of applying the novel tape scarfing method and indicates that laminates with the same strength may be achieved with a reduced ply drop spacing compared to conventional techniques. This is of significant benefit to weight critical designs, such as aircraft wings with numerous ply drop regions, where the potential to remove excess material quickly with minimal performance knockdown is highly desirable.

4. Analytical approach for delamination estimation

To gain some insight into the potential failure mechanisms, some simple calculations are presented. Although these involve a number of assumptions, they are useful in highlighting the relative importance of the different factors controlling failure. A fracture-mechanics based prediction of thick section delamination in tapered composites can be applied to the current test cases with conventional ply drops. The equation for calculating the strain energy release rate, G of a symmetrically tapered unidirectional laminate with a single ply drop on each side can be of the following form [2]:

$$G = \frac{\sigma_{thick}^2 ht}{4E_{11}(h-t)} = \frac{\sigma_{thin}^2 (h-t)t}{4E_{11}h} \tag{2}$$

where E_{11} is the longitudinal Young's modulus (164 GPa [10]), t is the thickness of the discontinuous plies on one side of the centre line, h is the thick section half thickness, G is the strain energy release rate (SERR) and σ_{thin} is the average stress in the thin section of the specimen. Rearranging for σ_{thin} and using a mode-II fracture toughness, G_{IIC} of 1.18 N/mm [16], the estimated failure stresses from Equation (2) for all conventional samples tested in this work are shown in Table 2. This value of G_{IIC} is slightly higher than reported elsewhere as it comes from a specimen with discontinuous plies, and thus includes the effect of compression enhancement - which is also relevant in the current case. For the scarfed samples the method was not applied since there is no discontinuity. As discussed in Ref. [17], some engineering judgement is needed when using this equation on interacting ply drops. Given that Equation (1) indicates the dropped plies in the 2 mm spacing specimen will be interacting and that the experimental results indicate that the interaction is as severe as in the 0 mm spacing case, it was assumed that the 2 mm spacing specimens act as a single large ply drop, as in the 0 mm case. As shown in Table 2, this approach yields reasonable correlation with the conventional specimens.

As an alternative approach, the simple and purely stress based method used in equation (1) was rearranged and trialled to estimate the delamination of the scarfed ply specimens, based on the assumption of interfacial shear failure at the scarfed ply end. To achieve this, the longitudinal stress carried in the discontinuous plies was assumed to be uniformly transferred to the continuous plies by shear stresses at the ply interfaces, as shown in Fig. 9. The triangular geometry at the scarfed discontinuous ply end was then idealised as a simple rectangle, as the length difference between the two interfaces is very small, e.g. L_{total} of 5 mm results in a ratio of $x/L_{\text{total}} = 1.06$. Then an expression was derived to estimate the expected failure stress of a given scarfed specimen based on the strength of the interlaminar resin region. The expected failure stress could thus be given by:

$$\sigma_{thick} = \frac{2L\tau_y}{t} \tag{3}$$

where L is the idealised length of the taper at the scarfed ply end, t is the total thickness of the discontinuous ply, $\tau_{y,}$ is the average interlaminar shear strength, measured using a double notched shear (DNS) specimen,

Table 2
Table comparing the accuracy in the estimated failure load for the experimental results based on idealised sample geometries using a simple shear-stress based method (eq. (3)), and a fracture mechanics approach. Lowest predicted failure stress in all cases is highlighted in green.

Sample Type	Spacing (mm)	Experimental Failure Stress (thin section) (MPa)	Failure from Shear Stress eq. (3) (MPa)	Failure from SERR eq. (2) (MPa)	Predicted fibre failure stress (MPa)**	Difference
Scarfed	**0**	**1511**	**1469**	–	2724	−2%
	2	**2064**	**2388**	–	2724	+16%
	5	**2611**	5143*	–	**2724**	−4%
Conventional	**0**	**1511**	–	**1313**	2724	−13%
	2	**1491**	–	**1313**	2724	−12%
	5	**2238**	–	**1922**	2724	−14%

* The failure mode was fibre failure. **The fibre direction laminate strength is 2724 MPa, according to Ref [10].

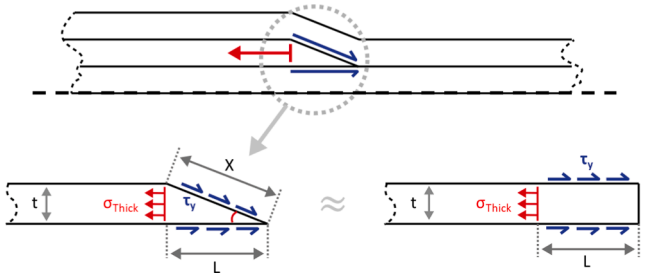

Fig. 9. Diagram of the assumed balance of forces and geometry at the ply drops in formulating equation (3).

and σ_{thick} is the average thick section stress, which can be simply converted to σ_{thin} based on the ratio of thicknesses. Using $\tau_y = 82.5$ MPa [11], $L = L_{total\text{-}measured}$ as shown in Fig. 2 for each specimen respectively, and $t = 0.786$ mm, which is the total thickness of the scarfed plies. The estimated stresses at failure for all of the scarfed ply samples tested in this work have been calculated as shown in Table 2. The failure estimations of this simple shear stress-based method were in reasonably good agreement with experimental values for the scarfed samples, considering the level of simplification. It must be noted that a very high delamination stress was estimated for the 5 mm spacing scarfed ply specimens, which could not be reached as those specimens failed by fibre failure. The fibre direction laminate strength is 2724 MPa, according to Ref. [10], whereas the experimental value obtained is slightly lower than that at 2611 MPa.

From these two simple analytical estimates, it becomes apparent that the conventionally dropped specimens' premature failure is well described as energy-based delamination, whereas the scarfed plies are better understood as shear stress dominated behaviour. Thus, the novel tape scarfing technique used in this work could allow for dramatically simplifying the laminate design process.

5. Numerical analysis

To gain ply-level stress distributions and a more fundamental understanding of how the scarfed ply drops change the stress distributions around the ply drop regions, numerical analyses were conducted based on a method previously demonstrated to accurately capture delamination type failures by multiple authors [18–20], which makes use of a custom written mesh generation code using the MATLAB software package.

5.1. FE model

Ply-by-ply 3D symmetric models of half the specimen thickness were created in ABAQUS/Explicit (ABAQUS, Simulia, US) consisting of a single element wide "slice" of solid elements representing each ply, with the interlaminar resin layer modelled using cohesive interface elements inserted between each ply. 8-node C3D8 solid elements were used with two elements through each blocked ply thickness, keeping an element aspect ratio of 1:1 as shown in the representative meshes shown in Fig. 10. At the discontinuous ply edge there is a transverse crack included - this has commonly been observed in experiments to occur at a far lower load than final failure [18]. Each model was 0.25 mm wide with all the nodes at the lateral faces constrained in the width direction to simulate a plane-strain stress state. The nodes at one end were fixed, with uniform displacements applied to the nodes at the other end horizontally at a constant rate of 0.25 mm/s. The mass was scaled up by a factor of about 1,000,000 to reduce run times. The dynamic effect was checked to be minimal by comparing the kinetic energy against the internal energy.

ABAQUS COH3D8 cohesive interface elements were used, incorporating a user-defined material subroutine VUMAT to simulate potential delamination in the inter-ply resin layer [20] – highlighted as red lines in Fig. 10. The thickness of the cohesive elements was set to zero. In the modelling of delamination using cohesive elements, both damage initiation, and then propagation criteria are used in the element formulation [22]. Fig. 11 shows a bi-linear traction displacement curve defining the behaviour of a cohesive element, where the point A is defined by the damage initiation criteria (strength of materials approach), and the area under the lines represents the damage

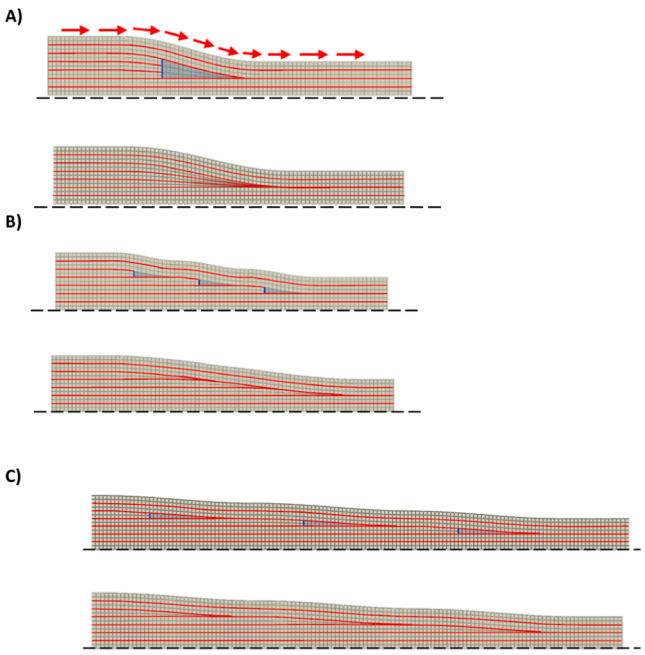

Fig. 10. Images of the meshes based on the cross-sectional photos included in Fig. 3, with conventional ply drops on top and scarfed plies bottom: (a) 0 mm ply drop spacing, (b) 2 mm ply drop spacing, and (c) 5 mm ply drop spacing. (Transverse cracks where present are highlighted in blue, and cohesive elements highlighted in red.)

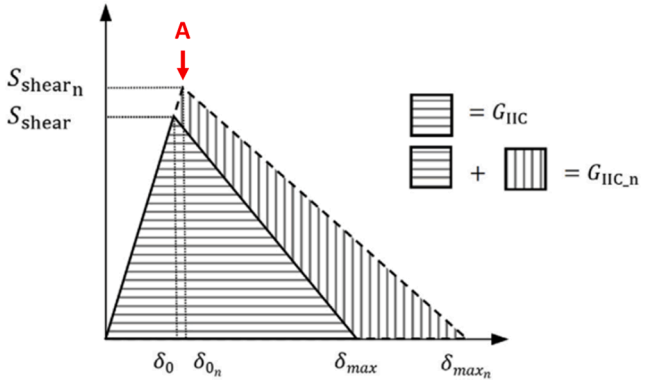

Fig. 11. Example of a Mode-II cohesive traction separation law, including the effect of TTC reproduced from Ref. [20]. δ_{max} and δ_0 are shear deformation at complete failure and initiation respectively. 'n' denotes enhanced values.

propagation behaviour (based on fracture mechanics). In the current study a stress-based damage initiation criterion assuming quadratic interaction between the through-thickness tensile stress (σ_{33}) and interlaminar shear stress (σ_{13}) was used, as described by Brewer and Lagace [21]:

$$\left(\frac{\langle\sigma_{33}\rangle}{\sigma_{33}^{max}}\right)^2 + \left(\frac{\sigma_{13}}{\sigma_{13}^{max}}\right)^2 = 1 \tag{4}$$

where $\sigma_{33}{}^{max}$ and $\sigma_{13}{}^{max}$ indicate the through-thickness strength S_{33} and shear strength S_{13}, respectively. An energy-based damage propagation model was employed, assuming a linear interaction between the contributions of Model I strain energy release rate, G_I and the Mode II strain energy release rate, G_{II} for damage evolution.

$$\left(\frac{G_I}{G_{IC}}\right) + \left(\frac{G_{II}}{G_{IIC}}\right) = 1 \tag{5}$$

It is well documented that through-thickness compression (TTC) enhances the interlaminar shear strength [23] and Mode II fracture energy [20,23,24] behaviour of composite laminates. A simple enhancement criterion outlined below in Equation (6) was applied to the current model based on the work of Xu et al. [20]:

$$\begin{cases} S_{13_n} = S_{13} - \eta_f \sigma_{33} \\ G_{IIC\_n} = G_{IIC}(1 - \eta_G \sigma_{33}) \end{cases} \tag{6}$$

where η_f is the TTC enhancement factor for interlaminar shear strength (S_{13}), and η_G is the enhancement factor for G_{IIC}. S_{13n} and G_{IIC_n} are the TTC enhanced values, and σ_{33} is the through-thickness compressive stress applied to the interlayer. Fig. 11 shows pictorially the effect of this enhancement criterion on the cohesive element response. The properties of the cohesive interface and continuum elements used are shown in Table 3, along with the enhancement factors. The properties chosen are identical to those presented in the literature defining the TTC enhancement law used in this work [20], except for the interface element strength parameters, which were chosen based on more recent studies [19,25]. The value of G_{IIC} chosen is 0.8 N/mm. Note that this is lower than the value applied in the simple analytical model in Equation (2) because it is the pure mode II value without the effect of any compression enhancement. For the curved belt plies, the material properties as included in Table 3 were oriented to follow the local axis of the continuum elements, as approximately shown by the red arrows in Fig. 10 (a).

Table 3
The modelling properties used in the finite element analysis presented in this work.

Properties of cohesive interface elements					
G_{Ic} (N/mm)	G_{IIc} (N/mm) [16]	S_{33} (MPa) [19]	S_{13} (MPa) [19]	n_f [23]	n_g (MPa^{-1}) [20]
0.2	0.8	90	110	0.3	0.064
Properties of continuum elements					
E_{11} (GPa)	$E_{22} = E_{33}$ (GPa)	$G_{12} = G_{13}$ (GPa)	G_{12} (GPa)	$\nu_{12} = \nu_{13}$	ν_{23}
164	11.4	5.17	3.98	0.32	0.436

S_{13} = out of plane shear strength, S_{33} = out of plane strength (peel)

5.2. Effect of ply scarfing on stress distributions at the ply drop region

Figs. 12 - 14 show the local stress distributions within the first layer of cohesive elements underneath the belt ply (highlighted in red) of each specimen. The distributions were plotted at the load that caused the first failure initiation for the conventional ply drop specimens – defined as

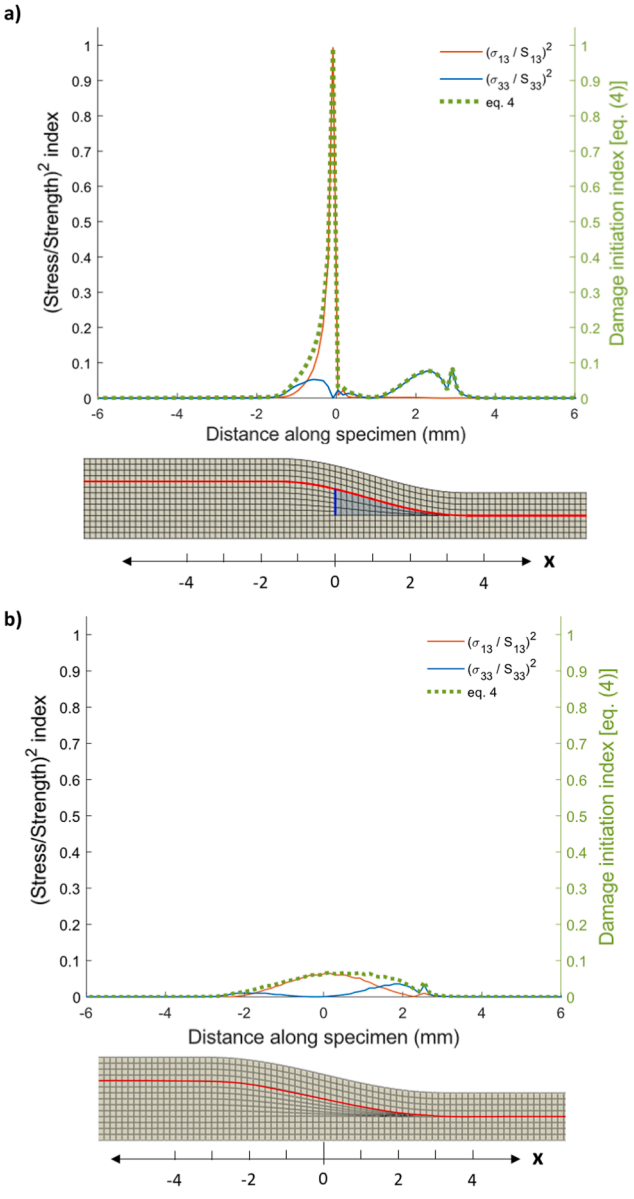

Fig. 12. Plot of the damage initiation criterion presented in Equation (4), along with its shear and peel stress components, taken at a stress of 370 MPa. All values were taken from the element centroids in the first layer of cohesive elements under the belt ply for: (a) the 0 mm spacing conventional model and (b) the scarfed model.

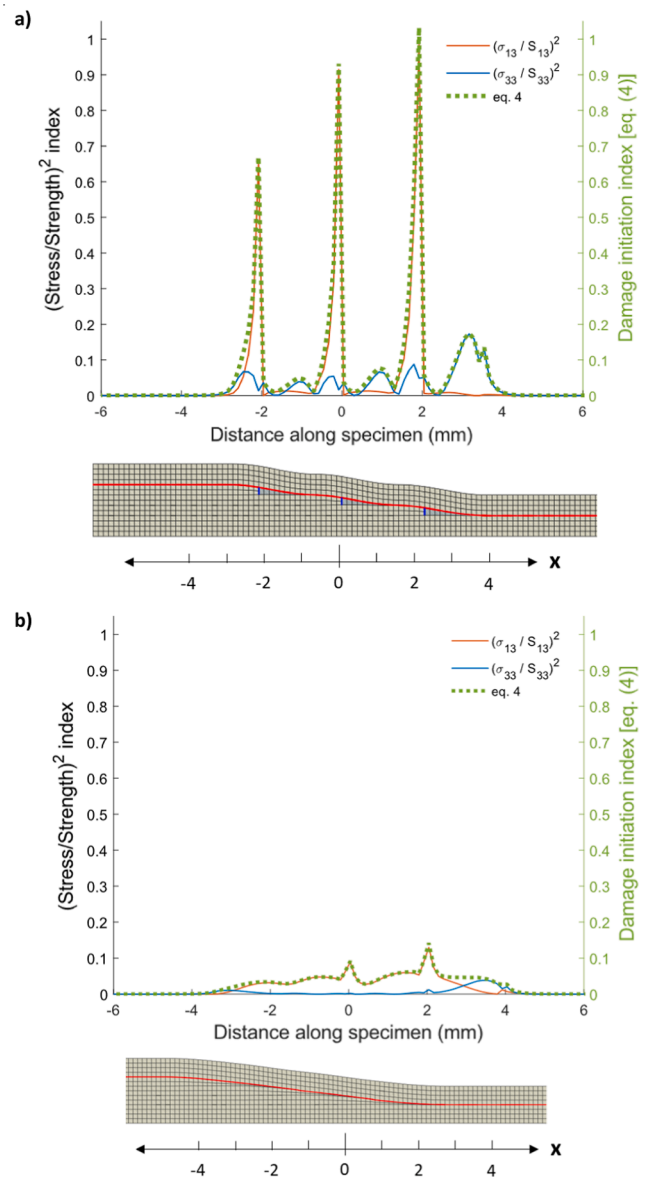

Fig. 13. Plot of the damage initiation criterion presented in Equation (4), along with its shear and peel stress components, taken at a stress of 620 MPa. All values were taken from the element centroids in the first layer of cohesive elements under the belt ply for: (a) the 2 mm spacing conventional model and (b) the scarfed model.

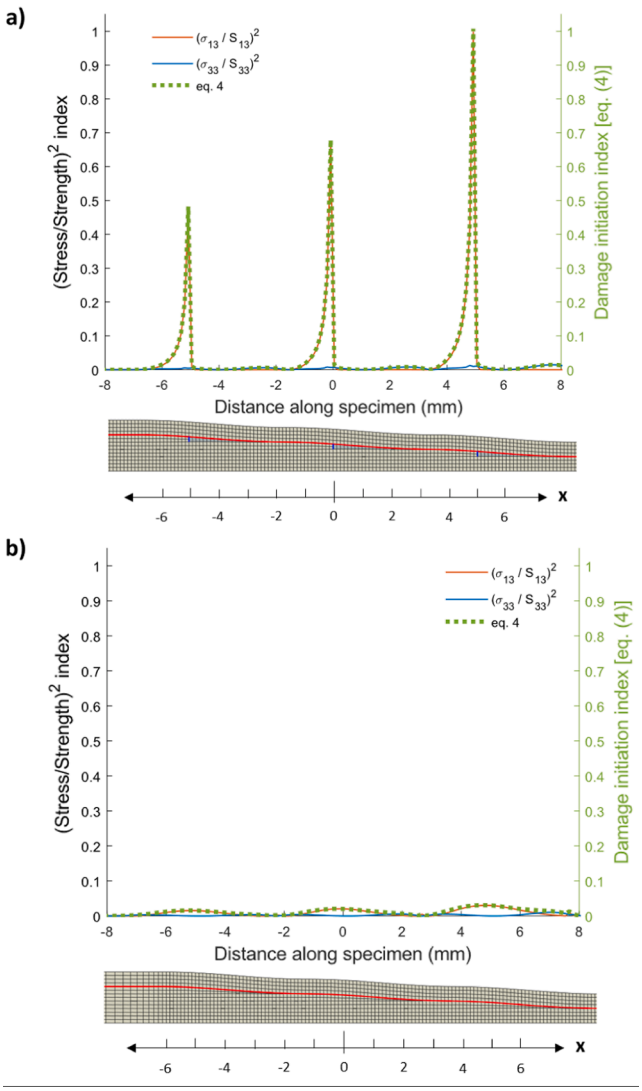

Fig. 14. Plot of the damage initiation criterion presented in Equation (4), along with its shear and peel stress components, taken at a stress of 630 MPa. All values were taken from the element centroids in the first layer of cohesive elements under the belt ply for: (a) the 5 mm spacing conventional model, and (b) the scarfed model.

when the initiation condition presented in Equation (4) is first met (point A in Fig. 11) – and show the clear difference in distributions between the different ply termination methods. The stresses were taken at the cohesive elements, and both the shear and the peel stresses in the elements have been normalised by their cohesive strengths, S_{13n} (as calculated by Equation (6)) and S_{33} respectively. They were both then squared and plotted on the same graph, indicating the contribution of either component of stress to the damage initiation criterion calculated using Equation (4). The value of the LHS of Equation (4) is also plotted in green on the second y axis, indicating the location and distribution of elements that have begun to take damage. For the scarfed ply specimens, this information is again plotted at the load level where at least one cohesive element in the conventional ply drop specimens was damaged to enable direct comparison.

In the conventional ply drop samples, the damage initiation index for all the specimens has highly localised sharp peaks, aligned well with the resin pocket. For the 0 mm spacing model, the maximum value of the damage initiation index has reached a value of 1 only in a single concentrated peak, with the rest of the specimen having a value close to zero. The peel stress contribution (blue line) to the initiation of failure is minor, with the shear stress providing the major contribution (orange line). Similarly, the 2 mm spacing model has highly localised damage initiation peaks corresponding to the heel and toe of each resin pocket, with very low values of initiation stresses outside of these regions. Failure initiated at the heel of the resin pocket closest to the core plies. The 5 mm spacing model continued the pattern present in the 0 mm and 2 mm spacing samples, with a very low ambient stress state and highly localised failure initiation peaks around the end of the dropped plies. In both the 2 mm and the 5 mm spacing samples, adjacent ply drops are contributing individual, non-intersecting peaks to the initiation of failure, and the material between them is at very low stress levels. Given that each of the conventional configurations failed with very high local stresses but with very low stresses in the surrounding material, the behaviour is indicative of energy dominated failure; the material surrounding the peak regions does not have high enough stresses present for the onset of damage, and the propagation of a crack will be dominated by the release of energy as new surfaces are formed.

In the scarfed ply drop samples, the damage initiation stresses along with the contribution of both peel and shear to failure initiation was much more diffuse than that in the conventional case. At the same load, the maximum peak initiation stress in the scarfed 0 mm spacing model was significantly lower than in the conventional 0 mm spacing model, and well below a failure index of 1. For the scarfed 0 mm spacing sample, the broad distribution to the damage initiation peak shows that a larger area of the specimen is under stress when compared to the conventional sample. For the 2 mm spacing model, which failed by delamination, the trend continues with much higher ambient stress levels surrounding the scarfed ply drops than were present for the conventional specimens, taking the form of a broad distribution dominated by its shear contribution. The 5 mm scarfed spacing model has three very broad and low peaks of stress located around each scarfed ply drop, far enough apart to be completely non-overlapping, each dominated by its shear contribution. The damage initiation index of each peak in this specimen is significantly lower than 1, an observation in line with the absence of delamination present, as these samples failed by fibre failure. In the scarfed specimens, the ambient stresses around the dropped plies were higher than those in the conventional specimens, which means that when the first element failure occurs, the surrounding material is likely to be at, or close to sufficient stress to enter the damaged state. This difference in stress distribution to the conventional configurations is clear in all samples - even at 0 mm spacing which was modelled with a small resin pocket present - and indicates that the failure of the scarfed specimens is stress dominated.

The observation of stress dominated behaviour for the scarfed plies, and the fact that the major contribution to the failure initiation is shear in all cases supports the simple analytical assumptions for thick section type delamination as presented in Equation (3) and explains how it provides a reasonable estimate for the failure stress. However, it is clear from all plots that the distributions of stress were not uniform, which highlights one source of approximation in Equation (3).

For the scarfed ply models, as shown in Figs. 12–14 the stresses contributing to delamination were spread over a larger area, without localised peaks triggering crack propagation. This resulted in a higher load carrying capacity and a lower sensitivity to the localised crack initiations.

As the ply drop spacing is increased, the stress peaks also become further apart. It is of note that in the scarfed 5 mm spacing model, the stressed regions are not intersecting, indicating that the terminated plies worked individually without interaction. This is concordant with both Equation (1), and the observation that the failure loads of 5 mm spacing and infinite spacing (or single ply drop) specimens were effectively the same.

5.3. Failure prediction

A comparison of the FEA simulations and experimental failure loads is shown in Fig. 15, with the failure modes found in Table 4. The point of failure in all cases that delaminated was chosen as the maximum load prior to load drop in the load–displacement output, as has been chosen previously [26], which also closely corresponded to the first complete failure of a cohesive element in each model, predicted based on Equation (5). For the scarfed 5 mm spacing specimen that failed via fibre failure, a simple maximum stress criterion was applied by post-processing the load displacement output from the model. When the average nominal thin-section tensile stress exceeded the tensile strength value of 2724 MPa, fibre failure was assumed to have occurred.

The difference between the failure loads of the FEA and the experiments in delamination prediction was lower than 11% in 4 out of the 5 models that failed in this manner, and within 16% in the worst case (2 mm spacing scarfed), as shown in Table 4. In all models, the failure mode was also in good agreement with the experiments, with the observation of rapid and unstable delamination growth into both the thin and thick sections for all 2 mm and 0 mm spacing configurations.

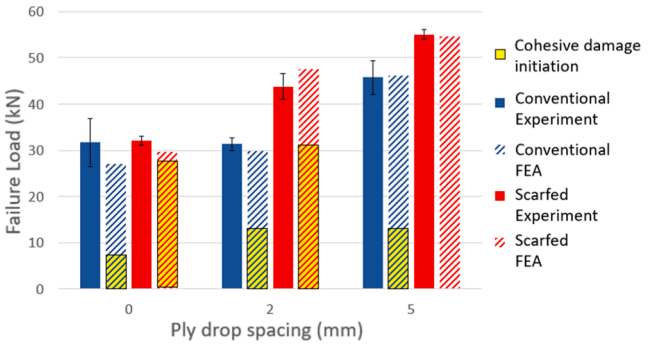

Fig. 15. Bar chart showing the average experimental failure load of all specimens tested (block colour) correlated with the expected failure predicted using the FEA (striped). The load at which cohesive damage initiation was satisfied (eq. (4)) is highlighted in yellow.

The delaminated region was identifiable clearly in the model, based on the location of cohesive elements which had undergone complete degradation. Whilst the FEA result provides an improvement in correlation to the test results for conventional ply drop specimens, over the simple SERR method presented in Equation (2), the SERR analytical model works well given an appropriate choice of G_{IIC}. A higher value is needed because G_{IIC} is affected by the through-thickness compressive stress - an effect which is captured by the TTC enhancement law in the FEA. This phenomenon has been previously commented on in detail in Ref. [2].

6. Conclusion

In this work a tape scarfing method that can apply a tapered profile with 1:20 aspect ratio (approx. 3°) to dropped ply ends was used on unidirectional tapered laminate specimens. Three different ply drop spacings (0 mm, 2 mm, and 5 mm) were applied to symmetrically tapered laminates with three successively dropped internal plies. The relationship between the spacing and the delamination behaviour in tensile loading was experimentally studied and compared with that of the same laminates with conventionally dropped internal plies. The reasons for the differences in failure mechanism were also investigated in greater depth using both analytical and numerical methods.

From the tensile test results, bringing successive ply terminations closer together in both configurations resulted in a decreased delamination stress, however the performance knockdown was significantly less when employing the tape scarfing technique:

- At 2 mm spacing, both failed by delamination, however the scarfed ply configurations failed at 38% higher load.
- At 5 mm spacing, the scarfed samples exhibited complete suppression of delamination and failed by thin section fibre failure. As a result, they were 17% stronger than the conventional specimens which failed by delamination.

Further to this, the delamination stress in the 2 mm spacing scarfed specimen (2064 MPa) is comparable to that of the 5 mm spacing conventional specimen (2238 MPa); reducing the spacing by 60% only resulted in 8% lower stress at failure when applying the tape scarfing method. This illustrates that the scarfing method can relax machine accuracy requirements or minimise the impact of the ply drop-off inaccuracy during manufacture, and reduce the ply drop spacing resulting in weight saving.

The analytical and numerical analysis showed that the delamination of scarfed ply specimens was determined largely by the overall interlaminar shear stress at the ply drop region, in contrast to the conventional ply drop specimens which were controlled by the highly localised peaks due to the discontinuities at the ply drops and were well predicted

Table 4
Correlation between FEA predicted failure and experimental result for all test specimens.

Sample Type	Spacing (mm)	Experimental thin section Failure Stress (MPa)	Failure mode (experiment)	Failure from FEA (MPa)	Failure mode (FEA)	% difference
Scarfed	**0**	1511	Thin + Thick	1481	Thin + Thick	−1.9
	2	2064	Thin + Thick	2377	Thin + Thick	+15.2
	5	2611	Thick	2724*	Fibre Failure	+4.6
Conventional	**0**	1511	Thin + Thick	1349	Thin + Thick	−10.7
	2	1491	Thin + Thick	1493	Thin + Thick	+0.2
	5	2238	Thick	2312	Thick	+3.3

using a fracture-mechanics based method. For the scarfed specimens with stress dominated behaviour, a simple expression assuming uniform stress distributions in the scarfed ply gave reasonable predictions of delamination onset stress (within 15%). This highlights the potential for simplifying the design process to optimise ply drop spacings. Using the detailed stress distributions that can be extracted from the FEA could help in further developing this approach.

CRediT authorship contribution statement

Tharan Gordon: Conceptualization, Methodology, Validation, Investigation, Writing – original draft, Data curation. **Xiaodong Xu:** Validation, Investigation, Writing – review & editing. **Luiz Kawashita:** Software. **Michael R. Wisnom:** Supervision, Writing – review & editing. **Stephen R. Hallett:** Supervision, Writing – review & editing. **Byung Chul Kim:** Conceptualization, Methodology, Writing – review & editing, Supervision, Project administration, Funding acquisition.

Declaration of Competing Interest

The authors declare that they have no known competing financial interests or personal relationships that could have appeared to influence the work reported in this paper.

Acknowledgement

This work was funded by the EPSRC project “Novel Tow Termination for High-Quality AFP Production of Composite Structures with Blended Ply Drop-offs” (EP/P027288/1) and the EPSRC Centre for Doctoral Training (CDT) grant (EP/L016028/1). All data required for reproducibility are provided within the paper.

References

[1] He K, Hoa SV, Ganesan R. The study of tapered laminated composite structures: A review. Compos Sci Technol 2000;60:2643–57.
[2] Cui W, Wisnom MR, Jones M. Effect of step spacing on delamination of tapered laminates. Compos Sci Technol 1994;52:39–46.
[3] Allegri G, Kawashita LF, Backhouse R, Wisnom MR, Hallett SR. On the optimization of tapered composite laminates in preliminary structural design. Proc. ICCM17 Conf. 2009.
[4] Mukherjee A, Varughese B. Design guidelines for ply drop-off in laminated composite structures. Compos Part B Eng 2001;32:153–64.
[5] Fish J, Vizzini A. Determination of Ply-Drop Configurations. Elev. Vol. Compos. Mater. Des., 100 Barr Harbor Drive, PO Box C700, West Conshohocken, PA 19428-2959: ASTM International; 1993, p. 323-323–10.
[6] Khan B, Potter K, Wisnom M. Suppression of Delamination at Ply Drops in Tapered Composites by Ply Chamfering. J Compos Mater 2005;40:157–74.
[7] Gordon T, Xu X, Kawashita L, Kim BC. Novel Tow Termination Method For Delamination Suppression In Tapered Composite Laminates. SAMPE Eur. Conf. 2019, Nantes: 2019.
[8] Gordon T, Xu X, Wisnom MR, Kim BC. Novel tape termination method for automated fibre placement : Cutting characteristics and delamination suppression. Compos Part A 2020;137:106023.
[9] Wisnom MR, Dixon R, Hill G. Delamination in asymmetrically tapered composites loaded in tension. Compos Struct 1996;35:309–22.
[10] HexPly ® 8552 Epoxy matrix (180°C/356°F curing matrix). 2016.
[11] May M, Hallett SR. An assessment of through-thickness shear tests for initiation of fatigue failure. Compos Part A Appl Sci Manuf 2010;41:1570–8.
[12] Carrella-Payan D, Kawashita LF, Allegri G. Tensile Testing Characterization of Asymmetrically Tapered Composite Laminates. 18 TH Int. Conf. Compos. Mater. 2011:1–6.
[13] DeVlieg R, Jeffries K, Vogeli P. High-Speed Fiber Placement on Large Complex Structures. Proc Aerosp Technol Conf Expo 2007:1–5.
[14] Cemenska J. Automating AFP tuning using a laser sensor. SAE Tech Pap 2011:1–5.
[15] Cui W, Wisnom MR, Jones MI. Effect of through-thickness tensile and compressive stresses on delamination propagation fracture energy. J Compos Technol Res 1994;16:329–35.
[16] Kawashita L, Jones M, Trask RS, Hallett SR, Wisnom MR. Static and fatigue delamination from discontinuous plies - experimental and numerical investigations. Proc Int Conf Compos Mater – ICCM 17, 2009:1–17 .http://iccm-central.org/Proceedings/ICCM17proceedings/Themes/Behaviour/DELAMINATION/F9.10%20Kawashita.pdf.
[17] Petrossian Z, Wisnom MR. Parametric study of delamination in composites with discontinuous plies using an analytical solution based on fracture mechanics. Compos Part A Appl Sci Manuf 1998;29:403–14.
[18] Kawashita L, Jones MI, Hallett SR, Wisnom MR, Giannis S. High fidelity modelling of tapered laminates with internal ply terminations. 18th Int. Conf. Compos. Mater., 2011, p. 1–6. http://www.iccm-central.org/Proceedings/ICCM18proceedings/papers/Th35-1-AF0699.pdf.
[19] Zhang B, Kawashita LF, Jones MI, Lander JK, Hallett SR. An experimental and numerical investigation into damage mechanisms in tapered laminates under tensile loading. Compos Part A Appl Sci Manuf 2020;133:105862.
[20] Xu X, Wisnom MR, Sun X, Rev T, Hallett SR. Experimental determination of Through-Thickness Compression (TTC) enhancement factor for Mode II fracture energy. Compos Sci Technol 2018;165:66–73.
[21] Brewer JC, Lagace PA. Quadratic Stress Criterion for Initiation of Delamination. J Compos Mater 1988;22:1141–55.
[22] Hallett S. Predicting progressive delamination via interface elements. Delamination Behav. Compos., Woodhead Publishing; 2008, p. 367–86.
[23] Gan KW, Hallett SR, Wisnom MR. Measurement and modelling of interlaminar shear strength enhancement under moderate through-thickness compression. Compos Part A Appl Sci Manuf 2013;49:18–25.
[24] Li X, Hallett SR, Wisnom MR. Predicting the effect of through-thickness compressive stress on delamination using interface elements. Compos Part A Appl Sci Manuf 2008;39:218–30.
[25] Lu X, Ridha M, Chen BY, Tan VBC, Tay TE. On cohesive element parameters and delamination modelling. Eng Fract Mech 2019;206:278–96.
[26] Hallett SR, Green BG, Jiang WG, Wisnom MR. An experimental and numerical investigation into the damage mechanisms in notched composites. Compos Part A Appl Sci Manuf 2009;40:613–24.